Canadian Mineralogist
Vol. 30, pp. 1113-1126 (1992)

CHARACTERIZATION OF MULTIPLE SERPENTINIZATION, WOODSREEF, NEW SOUTH WALES

DAVID S. O'HANLEY[1]
Department of Mineralogy, Royal Ontario Museum, Toronto, Ontario M5S 2C6

ROBIN OFFLER
Department of Geology, University of Newcastle, Callaghan, New South Wales 2308, Australia

ABSTRACT

Three episodes of alteration of the Woodsreef harzburgite were identified based on cross-cutting relationships in outcrop and on mineral assemblages, textures and $\delta^{18}O$ values. The earliest alteration, which is spatially restricted to shear zones, produced tremolite, chlorite, talc and antigorite (tremolite assemblage; $\delta^{18}O = 7.6, 7.7‰$). This assemblage was subsequently overprinted by the widespread development of lizardite ± brucite ($3.5 < \delta^{18}O < 5.0‰$) during the first serpentinization event. Lizardite + brucite ($4 < \delta^{18}O < 6‰$), representing complete serpentinization of the harzburgite, was replaced by lizardite and chrysotile matrix textures ($3.7 < \delta^{18}O < 8.6‰$), associated with the formation of veins of chrysotile asbestos ($6 < \delta^{18}O < 7‰$), that formed during the second serpentinization event (serpentine recrystallization). Temperatures for serpentine recrystallization, calculated using $\delta^{18}O$ values from serpentine – magnetite mineral pairs, are 350° to 220°C, and indicate that serpentine recrystallization occurred while temperature was dropping, consistent with increasing $\delta^{18}O$ values in younger assemblages. Delayed hydration of enstatite resulted in the release of SiO_2 after brucite had formed from the hydration of olivine, such that the reaction brucite + SiO_2 + H_2O = lizardite operated and resulted in the destruction of brucite. Both polygonal serpentine and chrysotile asbestos veins oriented perpendicular to the serpentinization front represent fractures induced in completely serpentinized harzburgite by volume expansion accompanying its serpentinization. The formation of lizardite after olivine and its continued persistence during serpentine recrystallization is attributed to the preferential stabilization of lizardite (relative to chrysotile and antigorite) by Fe^{3+}.

Keywords: serpentinite, serpentine, recrystallization, kernel pattern, volume change, temperature of serpentinization, Woodsreef, Australia.

SOMMAIRE

Trois épisodes d'altération de la harzburgite de Woodsreef, en Australie, ont été identifiés selon les relations de contact à l'affleurement et les assemblages de minéraux, les textures, et les valeurs $\delta^{18}O$. L'altération précoce, qui se limite aux zones de cisaillement, a produit trémolite, chlorite, talc et antigorite (pour l'assemblage à trémolite, $\delta^{18}O = 7.6, 7.7‰$). Cet assemblage a subséquemment été oblitéré par un développement généralisé de lizardite ± brucite ($3.5 < \delta^{18}O < 5.0‰$) au cours du premier événement de serpentinisation. L'assemblage lizardite + brucite ($4 < \delta^{18}O < 6‰$), qui représente la serpentinisation complète de la harzburgite, a ensuite été remplacé par lizardite et chrysotile dans la matrice ($3.7 < \delta^{18}O < 8.6‰$), avec la formation de veines de chrysotile ($6 < \delta^{18}O < 7‰$), au cours d'un second événement de serpentinisation (recristallisation de la serpentine). Les températures de recristallisation, telles que calculées à partir des facteurs de fractionnement entre serpentine et magnétite, s'étalent entre 350 et 250°C; elles semblent indiquer que cette recristallisation a eu lieu pendant une chute en température, qui concorde avec une augmentation en $\delta^{18}O$ dans les assemblages plus tardifs. Une hydratation retardée de l'enstatite aurait causé la libération de la silice après la formation de la brucite par hydratation de l'olivine, de telle sorte que la réaction brucite + SiO_2 + H_2O = lizardite a eu lieu; elle aurait éliminé toute trace de brucite. La serpentine polygonale et les veines de chrysotile orientées perpendiculaires au front de serpentinisation représentent toutes deux des fractures dans la harzburgite complètement serpentinisée causées par une expansion du volume accompagnant la serpentinisation. La formation de lizardite aux dépens de l'olivine et sa persistance au cours de la recristallisation de la serpentine sont attribuées à la stabilisation préférentielle de la lizardite par le Fe^{3+} relativement au chrysotile et à l'antigorite.

(Traduit par la Rédaction)

Mots-clés: serpentinite, serpentine, recristallisation, texture en noyau, changement de volume, température de serpentinisation, Woodsreef, Australie.

---

[1]Present address: Department of Geological Sciences, University of Saskatchewan, Saskatoon, Saskatchewan S7N 0W0

INTRODUCTION

The Woodsreef lizardite – chrysotile serpentinite, which hosts the Woodsreef chrysotile–asbestos deposit near Woodsreef, New South Wales, Australia (Fig. 1), is significant to the study of serpentinization for two reasons. Firstly, it contains rare antigorite, which is the sole serpentine-group mineral stable above 260°C in the MSH system ($MgO–SiO_2–H_2O$), based on the calculated location of the chrysotile-out reaction: chrysotile = antigorite + brucite (Berman *et al.* 1986). If the Woodsreef serpentinite contains stable assemblages of minerals, and the MSH model is the correct one to describe phase relations among the serpentine minerals, then their temperatures of formation should be less than 260°C. This hypothesis could be tested using oxygen isotope thermometry on serpentine–magnetite pairs of known paragenesis. Secondly, the alteration patterns in outcrop and in thin section suggest that three temporally distinct events affected the serpentine protolith. The earliest event of alteration produced tremolite and chlorite, with rare talc and antigorite (hereafter called the tremolite assemblage) found in some partly serpentinized samples. Based on the predominance of tremolite and chlorite and the rarity of antigorite, the tremolite assemblage is considered to result from hydration rather than serpentinization as defined by O'Hanley (1991). Serpentinization is characterized by the predominance of either lizardite or antigorite in the alteration assemblage. The second event led to the inception of serpentinization. It produced a partly serpentinized harzburgite containing lizardite ± brucite mesh-rim textures with olivine mesh-centers and partly serpentinized enstatite. The tremolite assemblage also is replaced by lizardite ± brucite mesh-rim textures. The third event, and second stage of serpentinization, is called serpentine recrystallization (O'Hanley 1991); lizardite ± brucite mesh-rim textures were recrystallized to produce successively lizardite + brucite mesh-textures, lizardite hourglass and interlocking textures and, in some cases, chrysotile interlocking textures. The formation of veins of chrysotile asbestos occurred during this event. Chemical data were obtained to distinguish the two serpentinization events.

The presence of chrysotile asbestos at Woodsreef has been known since the end of the last century, but exploitation of the ore did not occur until 1918, and then only on a small scale (Proud & Osborne 1952). Subsequently, the Chrysotile Corporation of Australia Pty, Ltd., developed and mined the deposit from 1972 to 1982. Previous studies of the deposit have concentrated on the genesis of the asbestos deposit and the structures within it. No consideration was given to the role of the shear zones in the development of the serpentine minerals and textures (Proud & Osborne 1952, Glen & Butt 1981, Katz 1986).

EXPERIMENTAL TECHNIQUES

The terminology of Mercier & Nicolas (1975) is used for peridotite textures, and that of Wicks & Whittaker (1977), as modified by Wicks & O'Hanley (1988), is used for serpentinite textures. The serpentine minerals were identified using an X-ray microbeam camera using the procedures of Wicks & Zussman (1975). The X-ray experiments utilized Ni-filtered, Cu$K\alpha$ radiation during runs of 8 hours under vacuum. Whole-rock analyses were carried out by X-Ray Assay Laboratories, Toronto, using X-ray-fluorescence spectroscopy. Fused beads were used for major elements, and powder pellets were used for minor elements. H_2O^+, H_2O^- and FeO were determined by wet-chemical methods. Density was measured using a triple-beam balance, with the sample immersed in a 25°C water bath.

Mineral compositions were determined with a JEOL 840 SEM microprobe at the University of Newcastle, and a JEOL 8600 Superprobe at the University of Saskatchewan. Operating conditions at Newcastle were 15 kV and 25 nA; at Saskatchewan, they were 15 kV and 10 nA. Natural mineral standards were used in both cases.

The serpentine textures at Woodsreef are dominated by one serpentine mineral and magnetite, which were separated from the samples using heavy liquids, an ultrasonicator and a magnet. The mineral separates are considered pure, with the exception being lizardite + brucite, which could not be separated. Oxygen was extracted from the minerals using the BrF_5 technique of Clayton & Mayeda (1963). The gas fraction was analyzed using a Finnigan Mat 251 isotope ratio spectrometer at the University of Saskatchewan. The data are reported using the δ notation in ‰ relative to Standard Mean Ocean Water. A $\delta^{18}O$ value of 9.6‰ was measured for the NBS quartz standard, which has an accepted value of 9.439‰.

GEOLOGICAL SETTING

The Woodsreef serpentinite is one of several serpentinite bodies that delineate the Peel – Manning Fault System (PMFS), a suture that extends for approximately 270 km near the western margin of the Southern New England fold belt (Fig. 1). The PMFS separates Devonian to Carboniferous forearc basin sequences of the Tamworth belt to the west from Silurian and Late Devonian – Early Carboniferous accretionary–subduction complex sequences of the Tablelands Complex to the east (Aitchison 1988, Blake & Murchey 1988, Ishiga *et al.* 1988). The Woodsreef serpentinite lies within a thin (< 4 km) belt of rocks that represent a dismembered ophiolite, located between the above two terranes. The presence of serpentinite detritus in Early Permian sedimentary rocks associated with rift basins that unconformably overlie both the Tamworth belt and the Tablelands Complex indicates that serpentinization had been

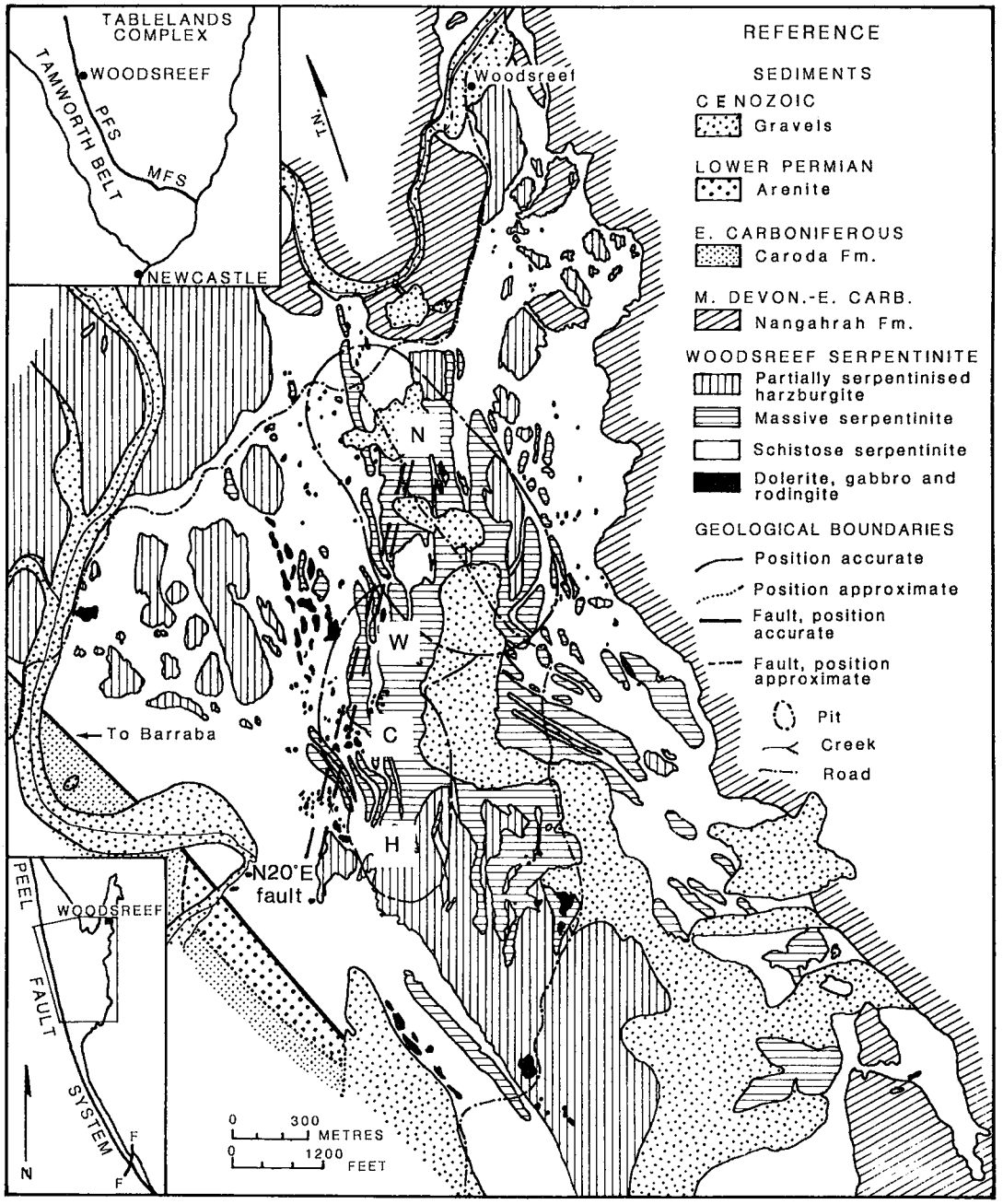

FIG. 1. Geology of the Woodsreef serpentinite in New South Wales. PFS: Peel Fault System, MFS: Manning Fault System. The inset in the lower left-hand corner shows the shape of the Woodsreef serpentinite and its setting with respect to the PFS. The N20E fault cuts across the northwestern parts of the open pits, labeled H (Hardie), C (Centre), W (Wunderlich) and N (North). Massive serpentinite on the map shows mainly a kernel pattern (shown in Fig. 2a), and occurs southeast of the N20E fault.

initiated before the Early Permian (Leitch 1988). However, serpentinization may have continued after this period. The presence of Tertiary sedimentary rocks containing serpentinite boulders on top of the Woodsreef serpentinite, and of a horizon of extensive weathering produced at the expense of serpentinite underneath the Tertiary rocks (Butt 1979), indicates that serpentinization had ended by the Tertiary at the latest.

The Woodsreef serpentinite is bounded on the west by the PMFS and on all other sides by the Nangarah Formation (Fig. 1; Blake & Murchey 1988). All contacts are vertical or steeply dipping to the east or west. The serpentinite is dissected by shear zones that consist of partly to completely serpentinized, block and matrix *mélange*, serpentine schist, rodingite and rodingitized dolerite (Scheibner & Glen 1972). The most important shear zone with regard to serpentine recrystallization strikes N20°E and dips 70°SE and is termed the N20E fault (Fig. 1). The strike and location of the fault suggest that it continues into the offshoot of the serpentinite to the northeast of the mine. All the asbestos mineralization occurs to the southeast of this structure (Glen & Butt 1981); the asbestos is found in veins that cut massive serpentinite and that are associated with narrower shear zones that vary in strike from 350° to 020°.

Patterns in Outcrop

The vast majority of the Woodsreef body consists of either massive or schistose, partly serpentinized harzburgite (Fig. 1). Massive serpentinized harzburgite is found only southeast of the N20E fault, and there it occurs mainly as a mantle surrounding a core of partly serpentinized harzburgite; this relationship is called "kernel" pattern (Fig. 2a). The boundary between partly and completely serpentinized peridotite is very sharp: it

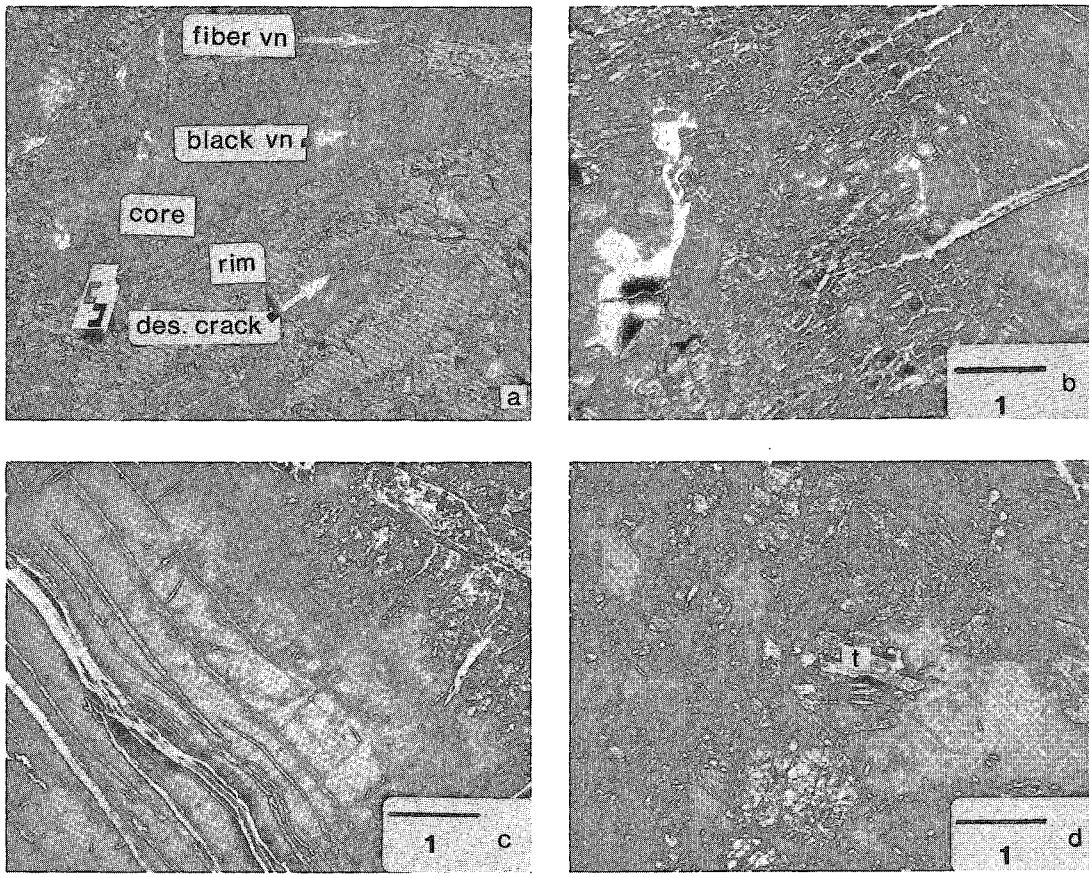

FIG. 2. a. Outcrop photograph from the Woodsreef mine, illustrating the details of the kernel pattern, which consists of partly serpentinized peridotite (in the core) mantled by completely serpentinized peridotite (rim). The core is cut by black veins (black vn). Asbestos veins (fiber vein) are located within the rims, whereas "desiccation cracks" (des. cracks) are located at the rim – core boundary of the kernel. Notebook is 25 centimeters high. Figures 2b to 2d are all photomicrographs, with scale bars in millimeters. b) Core – rim boundary of the kernel in sample W3. On the far right is lizardite hourglass texture, cut by a cross-fracture. In the middle is lizardite + brucite mesh-texture, with a wormy enstatite (now bastite) – chromite intergrowth. c) Core – rim boundary of the kernel in sample W3. Lizardite + brucite mesh texture is in upper right-hand corner. It is replaced by lizardite hourglass texture, and the latter texture is replaced by lizardite + magnetite. A polygonal serpentine vein cuts through the lizardite + magnetite texture. d) Partly serpentinized peridotite showing tremolite (t) after enstatite. A zone of cataclasis is evident to the left of the tremolite (sample W65).

is usually less than 1 cm wide in outcrop (Fig. 2a) and a millimeter wide in thin section (Figs. 2b, c). The edge of the kernel rim is defined as the boundary between the lizardite + brucite mesh-rim texture, which is part of the kernel rim, and the lizardite ± brucite mesh-rim texture, which is part of the kernel core (the distinction between these two assemblages is given below in the section "Textural features, kernel rims"). The kernel pattern is best developed adjacent to the smaller shear zones southeast of the N20E fault and diminishes with increasing distance to the southeast, where only partly serpentinized peridotite is found [see Fig. 4 in Butt (1979)]. Therefore, the distribution of the kernel pattern, and the complete serpentinization of the harzburgite, are spatially related to the minor shear zones southeast of, and proximal to, the N20E fault. Completely serpentinized harzburgite without kernel pattern was found only near shear zones in the Wunderlich and North pits (Fig. 1).

Chrysotile asbestos veins more than a few centimeters across and up to tens of meters long are commonly present next to kernel rims, but they are never found in kernel cores. In addition to asbestos veins, massive, apple-green veins of polygonal serpentine occur in the center of some kernel rims. Both asbestos and polygonal serpentine veins are bounded by completely serpentinized harzburgite.

Cross-fractures

The kernel rim – core boundary is cut at a high angle by fractures generally several millimeters across and a few centimeters long, filled with either massive, apple-green polygonal serpentine or chrysotile asbestos. Most fractures are perpendicular to the core – rim boundary, but those fractures that are oblique to the boundary commonly show conjugate offsets. In outcrop, the fractures are oriented radially about the kernel, and the wider the kernel rim, the longer and wider the cross-fracture. Under the microscope, the cross-fractures pinch out in the partly serpentinized core (Fig. 2b) and widen into the rim. These veins were called desiccation cracks by Cooke (1936) and lattice veins by Glen & Butt (1981). We call them cross-fractures because they cut across the core – rim boundary.

Textural Features

Cores of the kernels

The presence in many samples of relict olivine and orthopyroxene showing a protogranular texture indicates that the serpentine protolith was a harzburgite tectonite (Fig. 2b). Rare pods of dunite and orthopyroxenite dikes also are intrepreted to have been present. Modal abundances in the harzburgite are 65 to 70% olivine, 30 to 25% enstatite, and 5% chromite. Grains of chromite may show an opaque rim, but otherwise it is unaltered. Both red and brown spinels are present, and the delicate enstatite – chromite intergrowths are preserved (Fig. 2b). In addition to the protogranular textures, partly serpentinized peridotites in the Wunderlich pit contain kinked olivine and orthopyroxene, commonly exhibiting undulose extinction and subgrains. In some samples, a myriad of closely spaced fractures are present, associated with grain-size reduction by comminution, giving the rock the appearance of a cataclasite (Fig. 2d).

Tremolite (Fig. 2d), talc and chlorite are minor minerals in some samples of partly serpentinized peridotite from all pits except the Centre pit. Their formation predates the appearance of lizardite in mesh-rim textures (Fig. 2d); lizardite is common in all samples of partly serpentinized harzburgite. Tremolite is bent but not recrystallized in one sample. Antigorite was found in only 3 of 80 thin sections; it thus appears to be virtually absent from the Woodsreef serpentinite. However, where it occurs, antigorite predates lizardite.

Lizardite ± brucite in mesh-rim textures is the most common alteration assemblage in the partly serpentinized cores. Brucite was not observed optically but was identified in some diffraction patterns. Lizardite-1*T* bastite after enstatite with partly-altered-domainal and partly-altered-patchy textures occurs in the partly serpentinized harzburgite.

Rims of the kernels

The kernel core – rim boundary is taken as the boundary between the lizardite ± brucite assemblage, which is part of the core, and the lizardite + brucite assemblage, which is part of the rim. Brucite appears abruptly in the latter assemblage over a distance less than a millimeter across, and in outcrop it is seen as a yellow-weathering zone several centimeters across. In contrast, in the lizardite ± brucite assemblage, brucite was not observed optically. As brucite appears abruptly, rather than gradually, in the lizardite + brucite assemblage, the two assemblages are taken to represent two distinct events of alteration, an early event that produced lizardite ± brucite, found throughout the Woodsreef serpentinite, and a later event that only produced lizardite + brucite, along with the other kernel–rim assemblages, southeast of the N20E fault.

The sequence in which the kernel–rim textures formed is clear because younger textures occur successively with increasing distance away from the kernel core and exhibit clear overprinting relationships. The textures and mineral assemblages are, from oldest to youngest (Fig. 2c): lizardite + brucite + magnetite mesh-textures, lizardite ± magnetite hourglass textures, and lizardite + magnetite interlocking textures. In some samples, chrysotile + magnetite interlocking textures that formed through recrystallization of lizardite are present. It is clear from observations under the micro-

scope that modal magnetite increases with increasing recrystallization of serpentine (Fig. 2c).

Near the shear zones, the lizardite ± magnetite hourglass texture and the chrysotile + magnetite veins that cut the hourglass texture are replaced by chrysotile + magnetite interlocking textures, indicating that both matrix and vein minerals were recrystallized. Veins of chrysotile asbestos that cut lizardite after enstatite (bastite) were not recrystallized, however, which resulted in isolated lenses of asbestos in bastite surrounded by chrysotile interlocking textures. The lenses were originally part of ribbon asbestos veins, which consist of several parallel veins, 1 to 2 mm wide.

In the kernel rims, completely serpentinized grains of bastite have uniform, domainal, patchy and "shaggy" textures. Only lizardite-1*T* has been identified in bastite in this study, but Glen & Butt (1981) reported chrysotile based on powder diffraction patterns. In this paper, we assume that all grains of bastite are composed of lizardite-1*T*.

The Relationship Between Outcrop Patterns and Textural Features

The relationship between the outcrop pattern and the serpentine mineralogy and textures observed in thin section is shown schematically in Figure 3. The outcrop pattern is similar in all of the pits, except that serpentine without kernel pattern is present in the Wunderlich pit. The mineralogy and textures of the harzburgite and serpentinite change systematically with distance away from the shear zones. Chrysotile interlocking textures with isolated lenses of fiber in bastite (labeled bastite-fiber in Fig. 3) are found only near the shear zones. Ribbon veins with lizardite hourglass textures are found further away from the shear zones. Chrysotile asbestos veins decrease in number and width away from the shear zones, and they are not present in kernel rims most distant from the shear zones, where only black-colored "veins" containing lizardite hourglass texture are found (Figs. 2d, 3).

These patterns indicate that both the extent of serpentinization and the extent of serpentine recrystallization increase as the shear zones are approached. The presence of plastically deformed olivine and orthopyroxene in the Wunderlich pit suggests that alteration and deformation began earlier and at higher temperatures than in the other pits, in which these features were not observed. In contrast, the tremolite assemblage is found in partly serpentinized harzburgite near several shear zones. Thus, the alteration and deformation of the peridotite are spatially and temporally heterogeneous, and spatially related to shear zones.

Mineral and Rock Compositions

The serpentinite protolith consists of olivine (Fo_{91}), enstatite (En_{92}) and magnesiochromite (Table 1), characteristic of harzburgite tectonites. These minerals and their compositions are consistent throughout the peridotite (Glen 1971). Lizardite that formed after olivine (Table 2, analyses 1, 2; shortened to 2–1, 2–2) seems

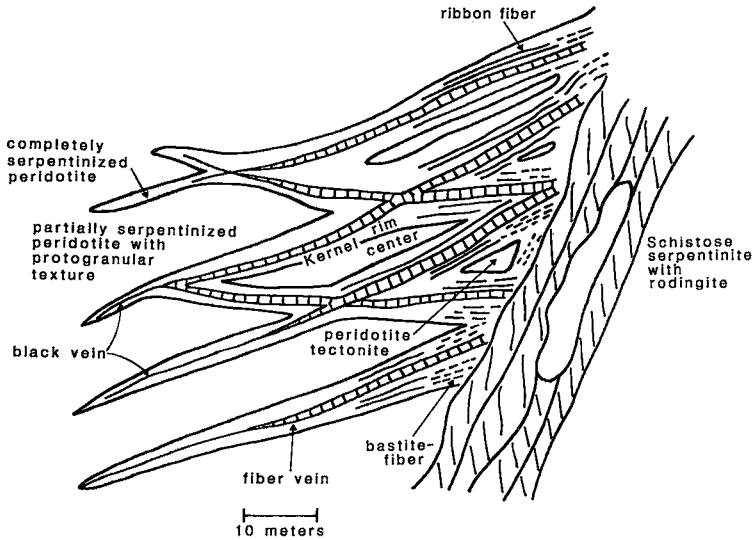

FIG. 3. Sketch diagram illustrating the spatial distribution of peridotite and serpentinite textures with respect to shear zones. Kernel pattern and asbestos veins are enlarged for clarity, but the horizontal scale is approximately correct.

TABLE 1. REPRESENTATIVE COMPOSITIONS OF MINERALS IN WOODSREEF SERPENTINIZED PERIDOTITE

		1 (4)	2 (2)	3 (2)	4 (2)	5 (2)
SiO_2	(wt.%)	40.55	38.96	56.46	0.36	0.32
TiO_2		0.01	0.03	<0.10	0.24	0.16
Al_2O_3		0.21	0.01	1.54	23.01	22.06
Cr_2O_3		0.15	0.03	0.75	45.80	47.29
FeO[1]		8.15	7.25	5.48	14.63	16.89
MnO		0.11	0.09	0.14	0.30	0.30
MgO		49.89	49.50	33.72	13.86	11.91
CaO		0.36	0.03	0.89	<0.08	<0.08
NiO		0.27	0.29	-	-	-
Na_2O		0.15	-	<0.14	<0.17	0.19
K_2O		0.07	-	<0.07	<0.07	<0.08
Total		99.92	96.19	98.97	97.93	99.13
Mineral Formula, using stated number of oxygen atoms		4	4	6	32	32
Si		1.00	0.99	1.96	0.08	0.08
Al		0.00	0.00	0.06	6.71	6.49
Cr		0.00	0.00	0.02	8.97	9.32
Fe		0.17	0.16	0.16	3.03	3.52
Mn		0.00	0.00	0.00	0.06	0.06
Ni		0.01	0.01	-	-	-
Mg		1.82	1.87	1.75	5.12	4.42
Ca		0.00	0.00	0.03	0.00	0.00
Fe/(Fe+Mg)		0.09	0.09	0.08		

1. olivine (sample W41). 2. olivine (W51). 3. enstatite (W51). 4. ferroan magnesiochromite (W41); 5. ferroan magnesiochromite (W51).
[1]total Fe as FeO. Numbers in parentheses represent the number of samples used in reported average. Compositions obtained from electron-microprobe data.

TABLE 2. REPRESENTATIVE COMPOSITIONS OF MINERALS IN WOODSREEF SERPENTINITE

	1 Lz[1] W41 (4)[2]	2 Lz, W51 (2)	3 Lz W41 (2)	4 Lz W41 (2)	5 Brc W41 (2)	6 Lz W51 (4)	7 Lz W41 (4)	8 Lz W51 (3)	9 Mag W51 (1)
(wt.%)									
SiO_2	37.79	36.92	39.13	38.99	0.30	41.31	39.90	39.73	0.73
TiO_2	0.01	0.00	<0.10	0.00	0.12	0.02	0.05	0.04	<0.12
Al_2O_3	0.18	0.10	0.92	0.78	0.12	0.45	0.50	0.76	<0.12
Cr_2O_3	0.05	0.04	0.87	0.69	0.10	0.10	0.06	0.45	0.42
FeO[3]	3.19	4.22	2.40	2.07	14.42	2.24	2.69	2.35	92.53
MnO	0.08	0.06	0.17	0.12	0.75	0.24	0.10	0.09	<0.13
MgO	41.05	39.90	38.66	39.95	50.38	39.82	39.08	39.91	0.60
CaO	0.08	0.03	<0.07	0.06	0.07	0.05	0.05	0.04	<0.08
NiO	0.22	0.35	-	0.03	-	0.02	0.11	0.07	-
Na_2O	0.15	-	<0.14	-	0.25	<0.14	<0.14	<0.14	<0.19
K_2O	0.07	-	<0.07	-	0.06	<0.07	<0.07	<0.07	<0.08
Total	82.87	81.62	82.53	82.69	66.57	84.64	82.75	83.65	94.28
Mineral Formula, using stated number of oxygen atoms	14	14	14	14	1	14	14	14	4
Si	3.78	3.75	3.90	3.87	0.00	3.97	3.96	3.93	0.04
Al	0.02	0.01	0.12	0.05	0.00	0.10	0.05	0.03	0.00
Cr	0.00	0.00	0.08	0.03	0.00	0.00	0.00	0.00	0.02
Fe	0.27	0.36	0.20	0.18	0.13	0.13	0.23	0.15	3.86
Mn	0.00	0.01	0.02	0.01	0.01	0.01	0.00	0.01	0.00
Mg	6.13	6.10	5.74	5.87	0.85	5.79	5.77	5.88	0.05
Ca	0.01	0.01	0.04	0.01	0.00	0.00	0.00	0.00	0.00

[1] (Lz = lizardite; Brc = brucite, Mag = magnetite, Ol = olivine)
1. & 2. Ol + Lz ± Brc zone. 3. bastite, Ol + Lz ± Brc zone. 4. bastite, Lz + Brc zone. 5. Lz + Brc zone. 6. Lz zone. 7., 8. & 9. Lz + Mag zone.
[2] Numbers in parentheses represent number of samples used to obtain average reported in table.
[3] Total Fe as FeO. Compositions obtained from electron-microprobe data.

richer in Fe than lizardite in recrystallized textures (*i.e.*, 2–6 to 2–9). However, the lizardite formed after olivine analyzed here contains high Mg and low Si pfu (per formula unit), features attributed to contamination by brucite. The brucite in the lizardite + brucite assemblage has an Fe/(Fe+Mg) value of 0.13 (2–5), significantly higher than the Fe content of all samples of lizardite in recrystallized textures. Lizardite after enstatite contains more Al and Cr and less Fe (expressed as FeO) and Mg than lizardite after olivine. Lizardite in recrystallized serpentinite contains less than 0.10 Al pfu and less than 0.03 Cr pfu (2–4, 2–6 to 2–8). There is no systematic change in total Fe, Al or Cr content with increasing degree of recrystallization. Magnetite also contains very little Al, Cr or Mg (2–9). The low Al and Cr values for lizardite after olivine and magnetite are attributed to the preservation of chromite and the low extent of recrystallization of lizardite after enstatite, the major sources of these cations in harzburgites.

A Mössbauer analysis of lizardite in the olivine + lizardite assemblage from mesh-rim textures shows that 40% of the Fe is Fe^{3+}, whereas lizardite from the lizardite æ magnetite hourglass assemblages has 50 to 72% Fe^{3+} (O'Hanley & Dyar, in press). These data indicate that the Fe^{3+} content of lizardite increases with increasing degree of recrystallization, with a slight decrease in total Fe as FeO based on electron microprobe analyses of comparable samples [from 3.19 (2–1) to 2.24 (2–6); Table 2]. O'Hanley & Dyar (in press) concluded, based partly on samples from Woodsreef, that the ratio of octahedrally coordinated Fe^{3+} to octahedrally coordinated Fe^{2+} in lizardite increases as modal magnetite decreases. The change in the $^{VI}Fe^{3+}/^{VI}Fe^{2+}$ ratio of lisardite is attributed to the exchange vector $Fe^{3+}_2Fe^{2+}_{-1}Si^{4+}_{-1}$. These observations can be described by the Fe end-member reaction:

$$Fe^{2+}_2Fe^{3+}_2SiO_6(OH)_4 + Si(OH)_4 + 0.33O_2 = Fe^{2+}_3Si_2O_5(OH)_4 + 0.33\ Fe_3O_4 + 2\ H_2O.$$

lizardite 1 = lizardite 2 + magnetite

Thus, the progress of serpentine recrystallization in the kernel rim, with a concomitant increase in modal magnetite, is attributed to an increase in $f(O_2)$.

Whole-rock compositions were obtained from nine assemblages in two samples that represent the transition from partly serpentinized harzburgite (Ol + Lz ± Brc; Table 3) to completely serpentinized harzburgite (Lz + Brc) to recrystallized serpentinite (Lz ± Mag, Lz + Mag). All compositions were renormalized to an anhydrous basis. Variations in Al_2O_3 and Cr_2O_3 are not considered because they vary sympathetically, and their values are low, suggesting that the presence or absence of chromite in the analyzed samples affects the reported values. The renormalized totals for the three samples of partly serpentinized harzburgite are virtually identical, so that they are represented on Figure 4 by a single point for the five parameters: SiO_2, FeO, MgO, Fe_2O_3 and total Fe (Fe^{tot}). These five parameters are plotted *versus* mineral assemblage, which represents increasing serpentinization and recrystallization to the right (Fig. 4).

The data in Table 3 for the transition from partly to

TABLE 3. WHOLE-ROCK COMPOSITIONS[1] AND ROCK DENSITIES FROM THE WOODSREEF SERPENTINITE, CONSISTING OF DIFFERENT MINERAL ASSEMBLAGES

	Ol+Lz± Brc[2] W41 (2)[3]	Lz+Brc +Mag W41 (1)	Lz+Mag W41 (1)	Ol+Lz± Brc W51 (1)	Lz W51 (2)	Lz+Mag W51 (2)
SiO_2	40.5	31.0	33.2	39.0	39.7	37.45
TiO_2	0.03	0.03	0.02	0.02	0.02	0.02
Al_2O_3	0.53	0.30	0.54	0.37	0.54	0.36
Cr_2O_3	0.35	0.26	0.68	0.25	0.36	0.16
Fe_2O_3[4]	3.56	7.62	3.42	3.61	3.78	8.60
FeO	4.00	-	2.60	4.00	0.90	3.25
MnO	0.14	0.19	0.13	0.13	0.13	0.10
MgO	40.2	43.0	42.70	41.00	39.80	36.00
CaO	0.80	0.11	0.06	0.33	0.10	0.07
Ni (ppm)	2750	3300	3000	3000	3150	2000
Na_2O	0.06	0.06	0.04	0.05	0.04	0.04
K_2O	0.06	0.06	0.06	0.06	0.06	0.06
P_2O_5	0.01	0.01	0.01	0.01	0.02	0.01
L.O.I.	9.43	16.8	16.7	11.0	15.55	13.3
Total	99.93	99.4	100.2	99.8	101.32	99.62
Density[5]	2.83	2.53	2.52	2.76	2.39	2.65

Rb, Sr, Y, Zr, Nb, Ba present in amounts < 32 ppm. L.O.I. = loss on ignition.
[1] Oxides expressed in wt. %.
[2] Minerals: (Ol)Olivine; (Lz)Lizardite; (Brc)Brucite; (Mag)Magnetite.
[3] Numbers in parentheses represent number of samples used in reported average.
[4] Fe_2O_3 represents total Fe unless a value is given for FeO.
[5] Density [gcm^{-3}] determined with a triple-beam balance and a water bath, at room temperature.

completely serpentinized harzburgite document a loss of CaO (from 0.8 to 0.11 wt.% for W41 and from 0.33 to 0.1 wt.% for W51), and an increase in L.O.I. (from 9.43 to 15.5 wt.% for W41 and from 11.0 to 13.3 wt.% for W51) during serpentinization. An increase in water content is consistent with the measured decrease in density accompanying hydration (Table 3).

During serpentine recrystallization, neither lizardite composition (Table 2) nor whole-rock densities (Table 3) change significantly. Although modal magnetite clearly increases with degree of recrystallization based on observations in thin section (Figs. 2b, c), the increase is small relative to the amount of lizardite present. Thus, the absence of clear compositional trends in the oxide data for the recrystallized assemblages is attributed to small variations in the modes that are not resolved in the whole-rock compositions.

A comparison of the data from the partly serpentinized rocks to those for the recrystallized rocks (Fig. 4) shows that the only consistent changes are a decrease in SiO_2 values and an increase in the Fe_2O_3/FeO ratio. These changes reflect a net change in the bulk composition of the harzburgite caused by two episodes of serpentinization. Although there is a net loss of SiO_2 during the two episodes of serpentinization, the absence of brucite from the recrystallized serpentinite in the kernel rim is attributed the oxidation of Fe^{2+} to Fe^{3+}, which stabilized magnetite instead of brucite, rather than a loss of MgO.

$\delta^{18}O$ Data for Serpentine and Magnetite

We obtained $\delta^{18}O$ data from samples containing representative assemblages of alteration minerals (Table 4) from serpentinite adjacent to two shear zones. Some samples of partly serpentinized peridotite, taken from the Wunderlich pit, contain the pre-serpentine tremolite assemblage (W65, W60). Other samples of partly serpentinized harzburgite from both the Hardie (W22, W51) and Wunderlich (W57) pits do not contain this assemblage.

The $\delta^{18}O$ data are plotted as a function of mineral assemblage within each shear zone, with the assemblages listed from oldest at the bottom to youngest at the top (Fig. 5). The youngest assemblages are invariably vein assemblages. The $\delta^{18}O$ data from partly serpentinized harzburgite can be divided into two groups: $\delta^{18}O$ values of 7.7 and 7.6‰ for samples containing the tremolite assemblage, and lizardite ± brucite; and $\delta^{18}O$ values less than 5.1‰ for samples containing lizardite ± brucite only. Completely serpentinized lizardite + brucite mesh textures have $\delta^{18}O$ values that vary from 3.7 to 5.9‰, which are slightly heavier than lizardite ± brucite assemblages in the same sample (*i.e.*, W51a to W51b; Table 4). Values of 3.7 to 7‰ for lizardite from the hourglass texture are similar to heavier than those from the lizardite + brucite mesh-rim texture in both shear zones. With the exception of the lizardite from the hourglass texture in sample W57c, successively younger assemblages in the kernel rim have heavier $\delta^{18}O$ values (Fig. 5).

Serpentine–magnetite mineral pairs were used for oxygen isotope thermometry (Table 4), using the empirical fractionation factor of Wenner & Taylor (1971). The locations of the serpentine–magnetite pairs in the paragenetic sequence are indicated by the calculated temperatures (Fig. 5). The matrix textures and veins, which formed during serpentine recrystallization, yield temperatures of 350° to 220°C (Table 4, Fig. 5). The calculated temperatures suggest that temperature decreased during serpentine recrystallization because serpentine–magnetite fractionations increase in later-formed veins.

Discussion

The relationship between the tremolite and lizardite ± brucite assemblages

The genetic relationship between the tremolite assemblage and the lizardite ± brucite assemblage in the kernel core that overprints it is not clear. The tremolite is deformed but not recrystallized, and is spatially related to shear zones, whereas lizardite ± brucite in partly serpentinized harzburgite is not. These differences suggest that the tremolite assemblage formed during a

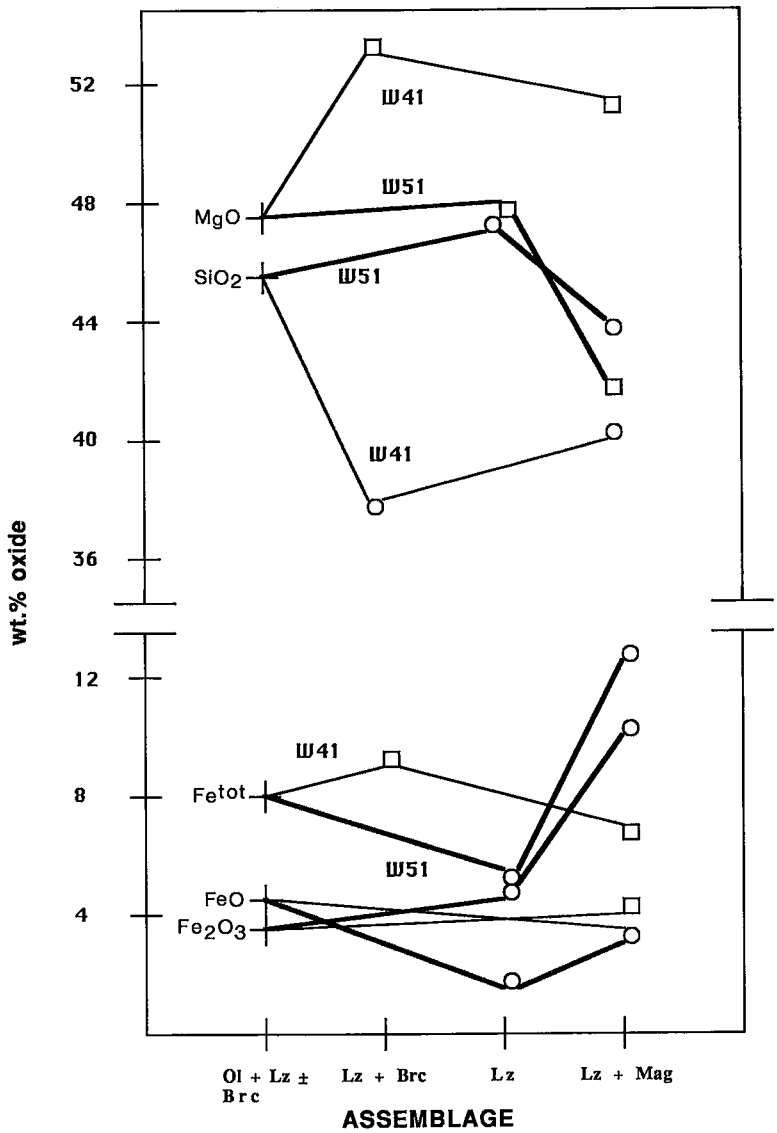

FIG. 4. Plot of whole-rock compositions (from Table 3) as a function of mineral assemblage. The extent of hydration and serpentine recrystallization increases from left to right. Bold lines represent compositions from sample W51, whereas light lines represent compositions from sample W41. Crosses represent compositions of samples of partly serpentinized peridotite.

different episode of fluid infiltration than lizardite ± brucite. Evaluation of the $\delta^{18}O$ data using the two end-member cases of chlorite (representing the tremolite assemblage) and lizardite-bearing assemblages reinforces this conclusion.

Chlorite and lizardite have markedly different isotopic compositions. This difference can be explained by a) crystallization of the minerals in equilibrium with the same fluid at different temperatures, b) crystallization of the minerals in equilibrium with the same fluid at different fluid/rock ratios, or c) crystallization of the minerals in equilibrium with different fluids. Although each of these explanations is theoretically feasible, two lines of evidence lead us to conclude that the third possibility is most applicable in this case.

Firstly, if lizardite formed at a lower temperature than chlorite at a constant water/rock ratio during the same event, then lizardite should be isotopically heavier than

TABLE 4. $\delta^{18}O$ DATA FOR WHOLE-ROCK SAMPLES[1] AND TEMPERATURES OF FORMATION OF CHRYSOTILE-MAGNETITE VEINS FROM THE WOODSREEF SERPENTINITE

	Sample	Assemblage[2]	$\delta^{18}O$ ‰	$\delta^{18}O_{Mag}$	T(°C)[3]
Hardie Pit	W22a	Ol + Lz, mesh	3.6		
	W41a	Ol + Lz, mesh	3.8		
	W51a	Ol + Lz, mesh	5.1		
	W41b	Lz + Brc, mesh	3.8		
	W47c	Lz + Brc, mesh	5.8		
	W51b	Lz + Brc, mesh	5.9		
	W41c	Lz, hrgls	5.5	-0.5	350
	W51c	Lz, hrgls	7.0		
	W51d	Lz, hrgls	6.2		
	W26c	Ctl, int	8.6		
	W47a	Ctl, int	6.0		
	W26a	Ctl, ribbon vn	6.4		
	W26b	Lz, banded vn	6.8		
	W47b	Ctl, asb vn	6.5		
	W47d	Ctl, asb vn	5.8		
	W51e	Ctl, asb vn	6.0		
Wunderlich Pit	W60a	Ol + Tr + Lz, mesh	7.7		
	W65a	Ol + Tr + Lz, mesh	7.6		
	W57a	Ol + Lz	4.0		
	W57b	Lz + Brc, mesh	5.0		
	W65c	Lz + Brc, mesh	4.7		
	W57c	Lz, hrgls	3.7		
	W60b	Lz, hrgls	6.4		
	W65d	Lz, hrgls	5.5		
	W66b	Ctl, asb in bastite	5.2	-1.7	300
	W67b	Ctl, asb in bastite	5.9	-0.8	300
	W66a	Ctl, int	6.2	-1.7	220
	W53	Ctl, int	6.4		
	W67a	Ctl, int	6.9		
	W68a	Ctl, int	7.3		
	W66c	Lz, banded vn	7.1		
	W60c	Ctl, asb vn	5.5		
	W68b	Ctl, asb vn	7.1		

[1] Samples arranged by pit and by paragenesis, from oldest at the top to youngest at the bottom

[2] Abbreviations are: olivine (Ol); lizardite (Lz); chrysotile (Ctl); brucite (Brc); tremolite assemblage (Tr). Textures are: vein (vn); interlocking (int); asbestos (asb); hourglass (hrgls)

[3] Temperature calculated using the fractionation factors of Wenner & Taylor (1971)

chlorite, because lizardite and chlorite have similar mineral–water fractionation curves (Wenner & Taylor 1971), and fractionation increases with decreasing temperature. However, the data indicate that lizardite is isotopically lighter than chlorite and therefore cannot be in equilibrium with the same fluid at a lower temperature. Secondly, if chlorite and lizardite formed isothermally at different water/rock values from a fluid that was isotopically lighter than unaltered peridotite, then lizardite would have formed at higher water/rock ratios than chlorite because lizardite has lighter $\delta^{18}O$ values than chlorite. However, chlorite has a higher $\delta^{18}O$ value than any measured for mantle peridotites [$\delta^{18}O$ values of 5 to 6‰; Wenner & Taylor (1974)]; at very low water/rock values, the $\delta^{18}O$ value of the precipitating mineral would be similar to that of the protolith, not heavier. Therefore, chlorite could not have formed at lower rock/water ratios and at the same temperature as lizardite from a fluid that was isotopically lighter than peridotite. Nor could lizardite and chlorite form isothermally at different water/rock ratios (chlorite at a high value and lizardite at a low value) from a fluid that is isotopically heavier than peridotite, because lizardite is isotopically lighter than peridotite, and could not form at very low water/rock values from peridotite. Thus, both geological and stable isotope data suggest that the tremolite assemblage and lizardite ± brucite did not form during the same event.

The relationship between the lizardite ± brucite and lizardite + brucite assemblages

The $\delta^{18}O$ values for the lizardite ± brucite assemblage in the kernel core are similar to slightly lighter than those for lizardite + brucite in the kernel rim. The data raise two possibilities for the relationship between the two textures. The first alternative is that the same fluid was involved in the formation of both textures, and that neither temperature nor water/rock value changed at the start of serpentine recrystallization. The second possibility is that two distinct fluids were involved in the formation of the two distinct mineral assemblages, and that the similarity in the $\delta^{18}O$ values is a result of recrystallization of lizardite ± brucite to lizardite + brucite at a temperature and water/rock ratio consistent with the observed $\delta^{18}O$ values. We prefer the latter alternative for two reasons. Firstly, the lizardite + brucite assemblage occurs in serpentinite found only in kernel rims southeast of the N20E fault. In contrast, the lizardite ± brucite assemblage is widespread. Secondly, in thin section, brucite is seen to appear abruptly in the lizardite + brucite assemblage, not gradually. If both assemblages were related to the same fluid event, it is expected that the assemblages would have the same spatial distribution and be related by a continuous variation in modes (O'Hanley 1991).

Successive mineral assemblages in the kernel rims have heavier $\delta^{18}O$ values, such that a trend toward heavier $\delta^{18}O$ values with increasing degree of serpentine recrystallization is evident (Fig. 5). The $\delta^{18}O$ data are consistent with cooling during recrystallization.

Formation of brucite

Although brucite is present in both partly and completely serpentinized peridotite at Woodsreef, it is not present in serpentinite in which the serpentine underwent recrystallization. Neither lizardite composition nor $\delta^{18}O$ values changed once brucite disappeared during recrystallization. Whole-rock compositions and densities of recrystallized rocks also are very similar. The only difference we have noted involves enstatite; it is partly to completely serpentinized in the kernel core and completely serpentinized to recrystallized in the kernel rims. These observations, and the absence of clear trends in the whole-rock data, suggest that elements were redistributed locally during the hydration event and early in the recrystallization event. However, based on the modal abundances of olivine and enstatite, only the addition of water, with neither a loss of Mg^{2+} nor a gain

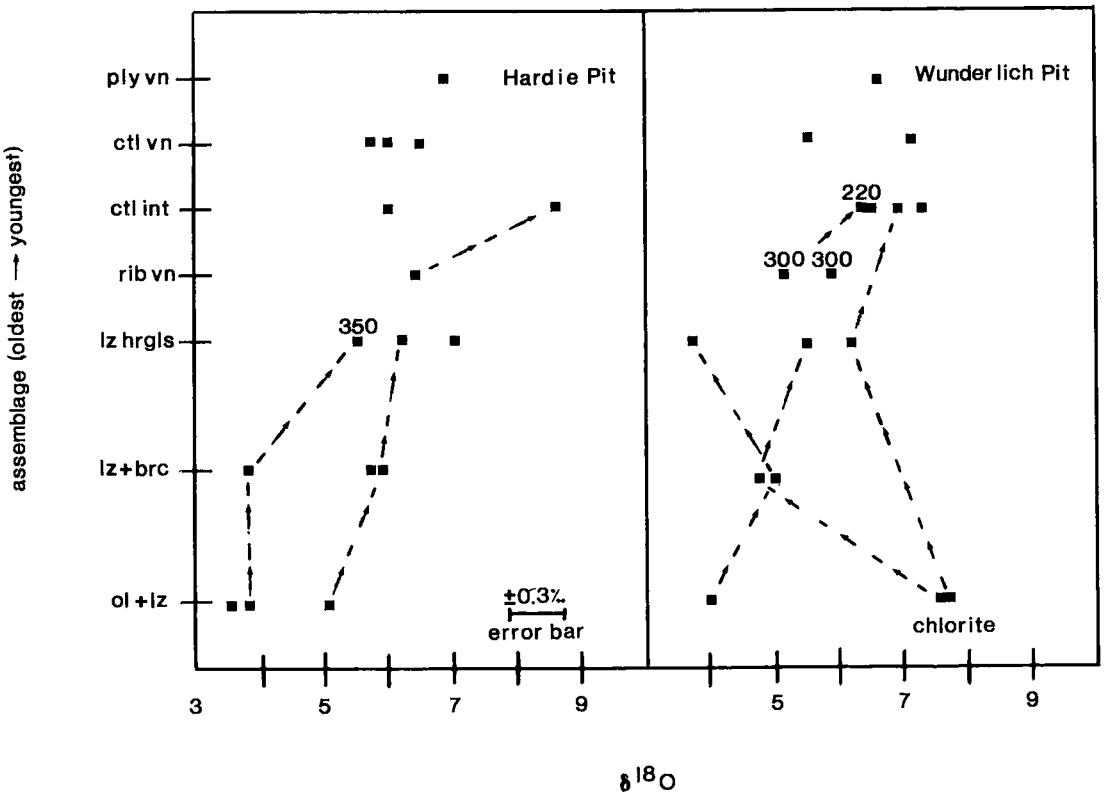

FIG. 5. Plot of measured $\delta^{18}O$ values *versus* associated mineral assemblage. Mineral assemblages are arranged from oldest at the bottom to youngest at the top. Temperatures of formation calculated by oxygen isotope thermometry are shown next to the assemblage on which they were determined. Dashed lines connect successive assemblages in one sample, with arrows pointing toward younger assemblages. The assemblages and textures are: (ol + lz): olivine + lizardite ± brucite mesh-rim, (chlorite): tremolite assemblage in ol + lz mesh-rim, (lz hrgls): lizardite hourglass, (lz + brc): lizardite + brucite mesh-texture, (rib vn): ribbon vein, or relict chrysotile asbestos within bastite, surrounded by chrysotile interlocking texture (ctl int); (chr vn): chrysotile asbestos vein, (ply vn): polygonal serpentine vein.

in $Si(OH)_4$, would be needed to form lizardite only. As enstatite reacted to form lizardite only, which suggests that a loss of Si from enstatite accompanied serpentinization, $Si(OH)_4$ is considered explicitly in the following reaction scheme to account for the mineral assemblages, using the MSH model:

1. 3 forsterite + 4.5 H_2O = 1.5 lizardite + 1.5 brucite (mesh textures);
2. enstatite + 1.33 H_2O = 0.33 lizardite + $Si(OH)_4$ (bastite textures);
3. brucite + 2 $Si(OH)_4$ = lizardite + 5 H_2O (hourglass textures);
4. 3 forsterite + enstatite + 3.33 H_2O = 2.33 lizardite (net reaction).

Enstatite reacted more slowly during hydration than did olivine, so that effectively, a dunite was hydrated initially, producing lizardite + brucite. As enstatite reacted, silica was made available for reaction with brucite to form more lizardite. The net reaction [reaction 4 = 1 + 2 + (0.5 × 3)] describes the conversion of harzburgite to a serpentinite without brucite.

The scheme of reactions shown above, in which brucite is totally consumed, would operate only in a serpentinized harzburgite with the appropriate ratio of olivine to enstatite. A rock with much less enstatite, such as a serpentinized dunite, would not contain enough silica to destabilize brucite. Completely serpentinized dunite would thus contain lizardite + brucite. Only one sample of completely serpentinized dunite (W80) was encountered during this study, and it consists of a lizardite + brucite interlocking texture, indicating that brucite did not react out in this rock during the recrystallization event. The presence of brucite in a recrystallized serpentinized dunite also argues for a local redistribution of elements during serpentinization.

Formation of cross-fractures

Based on Figure 1 of Hostetler *et al.* (1966), which permits the volume increase accompanying serpentinization to be calculated given the inferred ratio of olivine to enstatite and the observed ratio of serpentine to brucite, complete serpentinization at Woodsreef would have produced a 34% increase in volume. The cross-fractures are considered to be a manifestation of this volume increase.

Consider an interface between completely serpentinized peridotite and partly serpentinized peridotite undergoing hydration. Expansion accompanying serpentinization in the already partly serpentinized peridotite will expand the area of the interface occupied by it. However, the completely serpentinized peridotite cannot expand to match this increase and must fracture to accommodate it. The resulting fracture will be perpendicular to the interface, and the size of the fracture would equal the increase in area created by volume expansion accompanying hydration. With the next increment of hydration, expansion must recur, with consequent fracturing of the newly formed serpentinite. The existing fracture in the old serpentinite will widen further because it is farther away from the migrating interface. The space created by the widening fracture becomes a serpentine-bearing vein.

Instead of a one-dimensional interface, consider a box with serpentinization occurring on all six sides. Fractures will develop on all six sides, and their length and width will depend on how far into the box the serpentinization front has penetrated. The resulting pattern will consist of serpentine veins that cut the completely serpentinized peridotite but do not cut the partly serpentinized peridotite. The veins will be everywhere perpendicular to the core – rim interface, so that all veins will point into the center of the box. This is exactly the pattern shown by the cross-fractures.

The above argument applies to one kernel. However, at the 10-meter scale, the outcrop pattern is asymmetrical, with a greater degree of hydration and recrystallization near the shear zones and less farther away (Fig. 3). This pattern indicates that the shear zones were the fluid conduits during serpentine recrystallization. The outcrop pattern would also explain the varying width of the chrysotile asbestos veins, which are wider near the shear zones and taper to zero away from them (Fig. 3). If the boundary between the schistose and the massive serpentinite is considered to be equivalent to the core – rim boundary in the kernel, the chrysotile veins next to the kernel rims can also be considered to be cross-fractures.

Presence of chemical equilibrium

In the $MgO–SiO_2–H_2O$ system (MSH), all available data indicate that lizardite and chrysotile are polymorphs (O'Hanley *et al.* 1989). Within the MSH model, lizardite forms metastably from olivine, described by reaction 1 given earlier. Chrysotile is stable with antigorite below 260°C, whereas antigorite only is stable to 550°C at 2 kbars (Berman *et al.* 1986). Based on the MSH model, if chrysotile is stable at Woodsreef, then it should have formed at temperatures less than 260°C. As the calculated temperatures of chrysotile formation at Woodsreef are 300° and 220°C, with two values greater than 260°C, the temperatures are consistent with the stability field of chrysotile given the uncertainties in the thermodynamic data and the empirical isotope-based geothermometer.

However, at Woodsreef, lizardite + brucite mesh-textures and lizardite hourglass textures recrystallized to form new lizardite near 350°C (Table 4), suggesting that either lizardite is stable or else very persistent in its metastable state, although it is replaced by chrysotile in some samples. The recrystallization of lizardite in the supposed field of stability of antigorite can be explained in several ways.

Evans *et al.* (1976) placed the reaction chrysotile = antigorite + brucite at 300°C, *i.e.*, 40°C higher than the calculations of Berman *et al.* (1986), which are based on a different data-set. The reaction lizardite = antigorite + brucite is probably located at a lower temperature than the chrysotile reaction because of topological constraints on the reaction imposed by the locations of the reactions about invariant points (O'Hanley 1987). Given the uncertainty in the P–T coordinates of the chrysotile reaction and the uncertainty in the empirically derived thermometer, the two estimates of temperature are fairly close, and may be considered the same. However, this explanation does not account for the formation of lizardite rather than chrysotile; it only accounts for the persistence of lizardite once it forms.

A second possibility is that the calculated temperatures are too high. Although serpentine – water fractionation has not been determined experimentally [the experimental results of Sakai & Tsutsumi (1978) are rejected for the reasons stated by Kyser (1987)], the serpentine – magnetite model of Wenner & Taylor (1971) has yielded results consistent with the phase-equilibrium data, even though the thermometer is not calibrated. At Woodsreef, one calculated temperature is 220°C, which is within the stability field of chrysotile. Therefore, at present, we see no compelling reason to question the results of the thermometer.

A third possibility is that other cations affect the stability of lizardite and chrysotile with respect to antigorite, such that lizardite and chrysotile are stabilized at the expense of antigorite. Whittaker & Wicks (1970) suggested, on the basis of results of wet-chemical analyses, that the FeO/Fe_2O_3 ratio in lizardite (5 analyses; 0.28 ± 0.21) is less than that in chrysotile (6 analyses; 1.5 ± 1.24), and both are less than that in antigorite (3 analyses; 2.92 ± 1.68). Selective partitioning of Fe^{3+} into lizardite and chrysotile rather than antigorite would stabilize the former minerals at the expense of antigorite. For example, solubility of Fe^{3+} in chrysotile rather than

antigorite would change the MSH reaction chrysotile = antigorite + brucite to the $Fe^{3+}Fe^{2+}$MSH reaction; chrysotile = antigorite + brucite + magnetite, and stabilize chrysotile to higher temperatures. Mössbauer data on five samples of lizardite from Woodsreef, from both partly and completely serpentinized peridotite, contain between 40 and 72% Fe^{3+}, with total Fe as FeO between 2 and 3 wt.% (O'Hanley & Dyar, 1993). Chrysotile from asbestos veins in Woodsreef contains 2.5 to 3 wt.% Fe_2O_3, and 1.5 to 2 wt.% FeO based on six analyses (Glen & Butt 1981), so that both lizardite and chrysotile contain significant Fe^{3+}, with lizardite containing more Fe^{3+} than chrysotile. Therefore, we suggest that lizardite at Woodsreef is stabilized by the presence of Fe^{3+}. This conclusion implies that the MSH model is not appropriate to describe phase equilibria among the serpentine-group minerals at Woodsreef. Both Fe^{3+} and Fe^{2+} must be included in any thermodynamic model; however, the absence of solid-solution models for lizardite and chrysotile precludes such calculations at present.

Conclusions

Serpentinization of the Woodsreef peridotite occurred in two stages. The first stage is serpentinization, in which olivine, enstatite, and the tremolite assemblage were overprinted by lizardite ± brucite. The formation of the tremolite assemblage was not related to the formation of lizardite ± brucite. Recrystallization of serpentine during the second stage of serpentinization was controlled by a fluid emanating from the shear zones southeast of the N20E fault.

The $\delta^{18}O$ data for the alteration assemblages are consistent with the interpretation that three events of fluid infiltration affected the harzburgite. The first fluid produced tremolite, chlorite, talc and antigorite after olivine and enstatite. The second fluid produced lizardite ± brucite after all of the above minerals. Both alteration assemblages are found in partly serpentinized peridotite. The third fluid produced lizardite ± chrysotile ± magnetite from the earlier assemblages. It is manifest as kernel rims found southeast of the N20E fault. This interpretation is based on observations in outcrop and thin section. Although the temperatures during serpentinization are unknown, serpentine recrystallization occurred near 300°C, and temperature decreased during recrystallization. The formation of lizardite after olivine and the persistence of lizardite during serpentine recrystallization are attributed to the stabilizing affect of Fe^{3+} on lizardite. This conclusion indicates that the MSH model for the serpentine system is not fully appropriate to describe phase equilibria at Woodsreef, and that the ratio of ferrous to ferric iron in serpentine-group minerals must be considered in future models.

Acknowledgements

We thank Roger Laurent (Université Laval) and Thomas Chacko (University of Alberta) for their thorough reviews of the manuscript, and Robert F. Martin for his persistent fight for clarity in presentation. We also thank Roger Laurent, Kurt Kyser and Kevin Ansdell (University of Saskatchewan) for reading earlier versions of the manuscript. However, the conclusions are ours. We also thank Randy George (Department of Geological Sciences, University of Saskatchewan) for assistance with the electron microprobe, Edward Krupic and Walter Crebert (University of Newcastle) for preparation of thin sections and drafting of some of the figures, respectively. This work was supported by a Faculty Senate Research Grant, University of Newcastle, to R.O, and by an NSERC grant to T. Kurtis Kyser, who supported D.S.O. for some of the work.

References

Aitchison, J.C. (1988): Late Paleozoic radiolarian ages from the Gwydir terrane, New England Orogen, eastern Australia. *Geology* **16**, 793-795.

Berman, R.G., Engi, M., Greenwood, H.J. & Brown, T.H. (1986): Derivation of internally-consistent thermodynamic data by the technique of mathematical programming: a review with application to the system MgO–SiO_2–H_2O. *J. Petrol.* **27**, 1331-1364.

Blake, M.C., Jr. & Murchey, B.L. (1988): A Californian model for the New England foldbelt. *New South Wales Geol. Surv., Quarterly Notes* **72**, 1-9.

Butt, B.A. (1979): Exploration forecasts and exploitation realities at Woodsreef mine, New South Wales, Australia. *In* Geology of Asbestos Deposits (P.H. Riordon, ed.). *Soc. Min. Eng., Am. Inst. Min. Eng.*, 63-76.

Clayton, R.G. & Mayeda, T.K. (1963): The use of bromine pentafluoride in the extraction of oxygen from oxides and silicates for isotopic analysis. *Geochim. Cosmochim. Acta* **27**, 43-52.

Cooke, H.C. (1936): Asbestos deposits of Thetford district, Canada. *Econ. Geol.* **31**, 355-376.

Evans, B.W., Johannes, W., Otterdoom, H. & Trommsdorff, V. (1976): Stability of chrysotile and antigorite in the serpentinite multisystem. *Schweiz. Mineral. Petrogr. Mitt.* **56**, 79-93.

Glen, R.A. (1971): *The Geology of the Woodsreef Serpentinite, near Barraba, New South Wales.* B.Sc. Hons. thesis, Sydney Univ., Sydney, Australia.

_____ & Butt, B.A. (1981): Chrysotile asbestos at Woodsreef, New South Wales. *Econ. Geol.* **76**, 1153-1169.

Hostetler, P.B., Coleman, R.G., Mumpton, F.A. & Evans,

B.W. (1966): Brucite in alpine serpentinites. *Am. Mineral.* **51**, 75-98.

ISHIGA, H., LEITCH, E.C., WATANABE, T., NAKA, T. & IWASAKI, M. (1988): Radiolarian and conodont biostratigraphy of siliceous rocks from the New England fold belt. *Aust. J. Earth Sci.* **35**, 73-80.

KATZ, M.B. (1986): Tectonic analysis of the faulting at Woodsreef asbestos mine and its possible relationship to the kinematics of the Peel fault. *Aust. J. Earth Sci.* **33**, 99-105.

KYSER, T.K. (1987): Equilibrium fractionation factors for stable isotopes. *In* Stable Isotope Geochemistry of Low-Temperature Fluids (T.K. Kyser, ed.). *Mineral. Assoc. Can., Short-Course Handbook* **13**, 1-84.

LEITCH, E.C. (1988): The Barnard basin and the Early Permian development of the southern part of the New England fold belt. *In* Proceedings of the New England Orogen Symposium (J. Kleeman, ed.). Univ. New England, Armidale, N.S.W. (61-67).

MERCIER, J.-C.C. & NICOLAS, A. (1975): Textures and fabrics of upper-mantle peridotites as illustrated by xenoliths from basalts. *J. Petrol.* **16**, 454-487.

O'HANLEY, D.S. (1987): A chemographic analysis of magnesian serpentinites using dual networks. *Can. Mineral.* **25**, 121-133.

_____ (1991): Fault-related phenomena associated with hydration and serpentine recrystallization during serpentinization. *Can. Mineral.* **29**, 21-35.

_____, CHERNOSKY, J.V., JR. & WICKS, F.J. (1989): The stability of lizardite and chrysotile. *Can. Mineral.* **27**, 483-493.

_____ & DYAR, D. (1993): The composition of lizardite 1T and the formation of magnetite in serpentinites. *Am. Mineral.* **78** (in press).

PROUD, J.S. & OSBORNE, G.D. (1952): Stress-environment in 1T and the forma the genesis of chrysotile, with special reference to the occurrence at Woodsreef, near Barraba, New South Wales. *Econ. Geol.* **47**, 13-23.

SAKAI, H. & TSUTSUMI, M. (1978): D/H fractionation factors between serpentine and water at 100°C to 500°C and 2000 bar water pressure, and the D/H ratios of natural serpentines. *Earth Planet. Sci. Lett.* **40**, 231-242.

SCHEIBNER, E. & GLEN, R.A. (1972): The Peel thrust and its tectonic history. *New South Wales Geol. Surv., Quarterly Notes* **8**, 2-14.

WENNER, D.B. & TAYLOR, H.P., JR. (1971): Temperatures of serpentinization of ultramafic rocks based on $^{18}O/^{16}O$ fractionation between coexisting serpentine and magnetite. *Contrib. Mineral. Petrol.* **32**, 165-185.

_____ & _____ (1974): D/H and O^{18}/O^{16} studies of serpentinization of ultramafic rocks. *Geochim. Cosmochim. Acta* **38**, 1255-1286.

WHITTAKER, E.J.W. & WICKS, F.J. (1970): Chemical differences among the serpentine "polymorphs": a discussion. *Am. Mineral.* **55**, 1025-1047.

WICKS, F.J. & O'HANLEY, D.S. (1988): Serpentine minerals: structures and petrology. *In* Hydrous Phyllosilicates (Exclusive of Micas) (S.W. Bailey, ed.). *Rev. Mineral.* **19**, 91-167.

_____& WHITTAKER, E.J.W. (1977): Serpentine textures and serpentinization. *Can. Mineral.* **15**, 459-488.

_____ & ZUSSMAN, J. (1975): Microbeam X-ray diffraction patterns of the serpentine minerals. *Can. Mineral.* **13**, 244-258.

Received September 19, 1991, revised manuscript accepted January 8, 1992.